INORGANIC CHEMISTRY
FRONTIERS

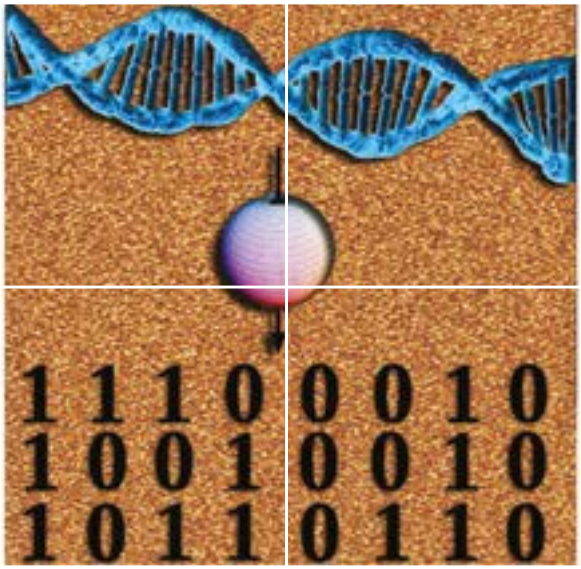

Accepted Manuscript

This article can be cited before page numbers have been issued, to do this please use: P. Du, X. Hu, X. Wang, C. Ma, M. du, J. Zeng, C. Jia, Y. Huang and R. Si, *Inorg. Chem. Front.*, 2017, DOI: 10.1039/C6QI00535G.

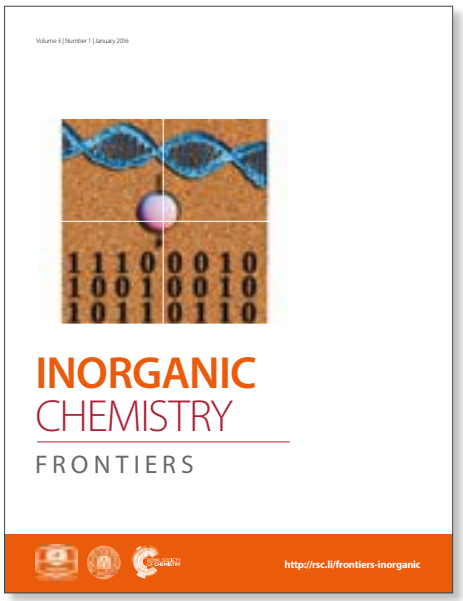

View Article Online
DOI: 10.1039/C6QI00535G

INORGANIC CHEMISTRY FRONTIERS

RESEARCH ARTICLE

Synthesis and Metal-Support Interaction of Subnanometer Copper-Palladium Bimetallic Oxide Clusters for Catalytic Oxidation of Carbon Monoxide

Received 00th January 20xx,
Accepted 00th January 20xx

DOI: 10.1039/x0xx00000x

www.rsc.org/

Pei-Pei Du,[a] Xiu-Cui Hu,[b] Xu Wang,[a] Chao Ma,*[c] Meng Du,[a,d] Jie Zeng,[c] Chun-Jiang Jia,*[b] Yu-Ying Huang,[a] Rui Si,*[a]

Subnanometer oxide clusters with distinct metal-support interaction have been attracted great interest due to their possible superiority in catalytic performance than conventional metal-oxide nanoparticles. In this paper, we report the solution-based chemical synthesis of a new type of copper-palladium bimetallic oxide clusters anchored to the surface of ceria nanorods. Revealed by the aberration-corrected high-angle annular dark-field scanning transmission electron microscopy (HAADF-STEM) and X-ray absorption fine structure (XAFS) techniques, we have identified that both copper and palladium species are fully oxidized with dominant metal-support interaction contributions by strongly bound M-O_x-Ce (M = Cu or Pd) structure. However, no direct bond between copper oxide and palladium oxide clusters, i. e. Cu-O_x-Pd, has been verified by experimental evidences, and thus no synergistic effect on the catalytic activity of bimetallic copper-palladium oxide clusters, compared to that of single metal (palladium) oxide clusters, has been demonstrated for the CO oxidation reaction.

Introduction

Nowadays, due to the limited resources available for energy conversion, chemical production, and environment protection, it is a great challenge to develop efficient heterogeneous catalyst with high activity and good stability. Recent studies demonstrated that subnanometer (< 1-2 nm) metal oxide clusters exhibit superiority in reactivity compared to the common nanoparticle (> 2 nm) counterpart.[1,2] Therefore, developing the fabrication of subnanometer catalyst with supported oxide clusters and deepening the understandings on the structure-activity relationship are significantly urgent in heterogeneous catalysis. A realistic approach via wet chemical method has been utilized to synthesize such oxide clusters for both noble metal (Au,[1,3] Pt,[4,5] Pd[6,7]) and transition metal (Fe,[8] Cu[9,10]) catalysts. Meanwhile, the important findings on theoretic calculation[11] can also provide new synthetic strategy. On the other hand, due to the synergistic effect[12,13], the bimetallic oxide catalysts usually behave superior reactivity than the related single metal oxide counterparts, probably originated from their tunable electronic and/or geometric structure.

However, till now, the studies on bimetallic oxide clusters are limited,[12,14] because very few preparation systems have been achieved and investigated. For wet chemical synthesis, the delicate control on the growth of as-formed poly bimetallic hydroxyls (or other anions) nuclei within the subnanometer scale is very tough. On the other hand, the precise and comprehensive detections on such disordered coordination structure are extremely difficult in experiments, which prevents us to further build the structure-activity relationship on these bimetallic oxide clusters. Multiple tentative approaches, including aberration-corrected high-angle annular dark-field scanning transmission electron microscopy (HAADF-STEM)[1,3-5] and X-ray absorption fine structure (XAFS)[3-5,8,10,12] have been used for bimetallic oxide clusters. However, the correlation between characterization results and catalytic performance of these subnanometer catalysts should be very careful to bypass any pseudo-phenomena or misleading conclusions.

In this work, we have prepared the ceria nanorods, which have been widely used in the preparation of single metal or metal oxide nanocatalysts (Au/CeO_2,[15] Pt/CeO_2,[5] Pd/CeO_2,[7] CuO_x/CeO_2,[10,16,17] etc.), as a reducible oxide support, and sequentially deposited both copper and palladium species via a deposition-precipitation approach. By the aids of HAADF-STEM and XAFS techniques, we have systematically investigated the local coordination structures around Cu and Pd atoms, comprehensively clarified the metal-support interaction in Cu-Pd-Ce-O system with the help of temperature-programmed reduction by hydrogen (H_2-TPR), and clearly uncovered the effect of secondary metal (Cu) oxide on the catalytic performance of single metal (Pd) oxide clusters. Specifically, no synergistic effect on the catalytic activity of bimetallic copper-palladium oxide clusters for oxidation of carbon monoxide, since no direct bond between copper oxide and

[a] Shanghai Synchrotron Radiation Facility, Shanghai Institute of Applied Physics, Chinese Academy of Sciences, Shanghai 201204, China.
[b] Key Laboratory for Colloid and Interface Chemistry, Key Laboratory of Special Aggregated Materials, School of Chemistry and Chemical Engineering, Shandong University, Jinan 250100, China.
[c] Hefei National Laboratory for Physical Sciences at the Microscale, University of Science and Technology of China, Hefei, Anhui 230026, China.
[d] Department of Chemistry, College of Science, Shanghai University, Shanghai 200444, China

View Article Online
DOI: 10.1039/C6QI00537C

palladium oxide, i. e. Cu-O_x-Pd, can be confirmed by our accurate structural detection.

Results and discussion

Table 1. Physical properties of ceria-supported copper-palladium oxide clusters.

Sample	Cu (at.%)	Pd (at.%)	S_{BET}[c] (m^2/g)	a[d] (Å)	D[d] (nm)
CuCe	4.2[a] 8.4[b]	—	96	5.4029(3)	8.6
PdCe	—	1.4[a] 2.9[b]	96	5.4117(2)	9.5
CuPdCe	4.4[a] 8.0[b]	1.4[a] 2.7[b]	88	5.4090(2)	9.7

[a] Bulk concentration by ICP-AES; [b] Surface concentration by XPS; [c] From N_2 adsorption/desorption; [d] From XRD.

Table 1 shows that the experimental data on bulk copper and palladium concentrations (Cu_{bulk}: 4.2–4.4 at.%; Pd_{bulk}: 1.4 at.%) are in good agreement with the designed values (Cu: 4.8 at.%; Pd: 1.6 at.%) for both bimetallic oxide sample (**CuPdCe**) and single metal oxide references (**CuCe** and **PdCe**). So, the deposition-precipitation approach is an effective synthesis to load metal ions on the surface of ceria nanorods. Meanwhile, Table 1 presents that the copper and palladium concentrations are in the range of 8.0–8.4 and 2.7–2.9 at.% for surface copper (Cu_{surf}) and Pd (Pd_{surf}) concentrations, respectively, nearly twice as high as the corresponding bulk concentrations. Thus, both copper and palladium species were majorly segregated on the surface of ceria nanorods.

Table 1 exhibits that the BET specific surface area of **CuPdCe** (88 m^2/g) is very close to that of **CuCe** or **PdCe** (96 m^2/g). Meanwhile, these numbers are similar to the reported value on pure ceria nanorods (80 m^2/g).[16] Fig. 1a displays that the Ce^{4+} components of u'''/u''/(u_0,u) and v'''/v''/(v_0,v) are dominant;[17] while the Ce^{3+} components of u' and v' are minor.[17] We found no observable differences on surface Ce^{3+}/Ce^{4+} ratios between bimetallic oxides and single metal oxide. Raman spectra (Fig. S1) show a F_{2g} peak at ca. 450 cm^{-1} and a weak band for defect site around 550~600 cm^{-1} for all the measured samples.[18] No significant differences on intensity of defect site band were observed between bimetallic oxides (**CuPdCe**) and single metal oxides (**CuCe** and **PdCe**). This is consistent with the XPS Ce 3d results that these catalysts share the same level of defective oxygen vacancies in air at room-temperature.

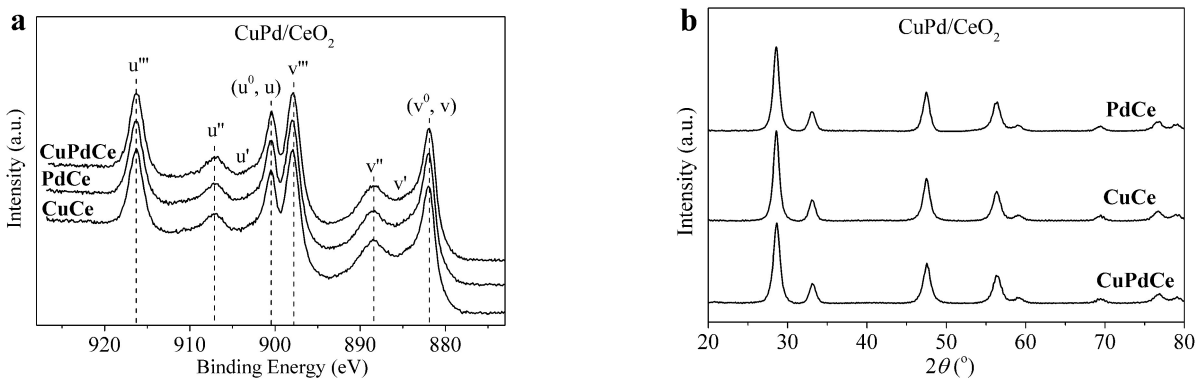

Fig. 1 (a) Ce 3d XPS spectra and (b) XRD patterns of ceria-supported copper-palladium oxides.

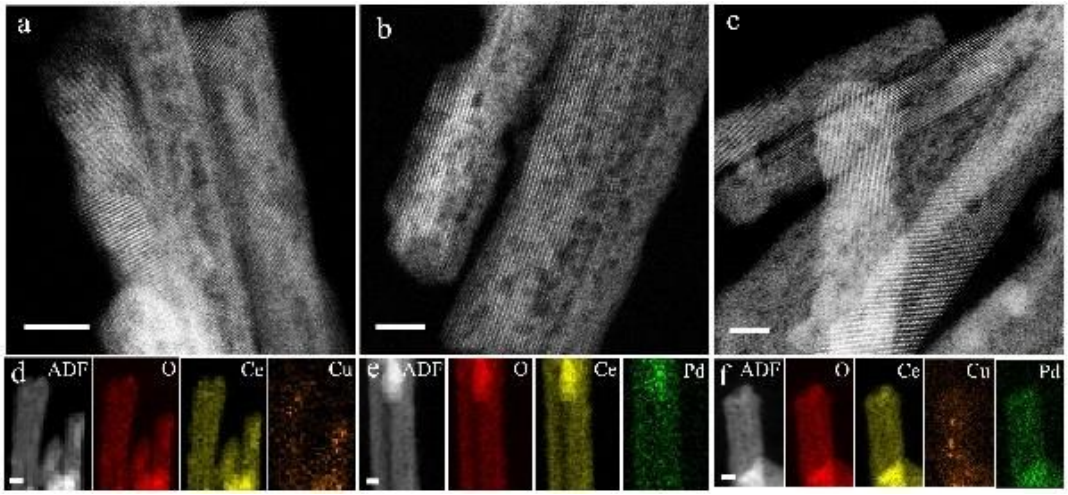

Fig. 2 (a–c) HAADF-STEM images and (d–f) the related EDS mapping results of ceria-supported copper-palladium oxides: (a,d) **CuCe**; (b,e) **PdCe**; (c,f) **CuPdCe**. Scale bars: 5 nm.

View Article Online
DOI: 10.1039/C6QI00535G

Fig. 1b represents a pure cubic Fluorite *fcc* CeO_2 (JCPDS card no.: 34-394) phase for all the measured samples, without any signals for $Cu/Cu_2O/CuO$ and Pd/PdO. Table 1 shows that the calculated lattice constants a of **CuPdCe** (5.4090 Å) and **PdCe** (5.4117 Å) are nearly identical to that of pure ceria support (5.4118 Å). 14 The slight decrease of a value for Pd-free sample (**CuCe**, 5.4029 Å) reveals that small fraction of Cu^{2+} ions may penetrate into the lattice of CeO_2 at the surface or sub-layer of nanorods. As discussed above, the ceria supports in both bimetallic oxide and single metal oxides share the same structural and textural properties.

Fig. 2a-2c confirm the *fcc* CeO_2 structure for both bimetallic oxide (**CuPdCe**) and single metal oxides (**CuCe** and **PdCe**). No lattice fringes for $Cu/Cu_2O/CuO$ or Pd/PdO were detected, which is well consistent with the XRD analysis. Furthermore, we observed a large number of surface voids for ceria nanorods, probably caused by the dehydration process during the growth of rod-like CeO_2 nanocrystals.[19]

Fig. 2d-2f exhibit that homogenous dispersion of Pd for either single metal oxide (Fig. 2e) or bimetallic oxides (Fig. 2f), but the Cu-rich microdomains with up to 1–2 nm in size are shown for both **CuCe** (Fig. 2d) and **CuPdCe** (Fig. 2f). Therefore, with the help of HAADF-STEM (spatial resolution: < 1 Å), we can identify that palladium species are uniformly distributed across the nanorod surface, in the particle-free form; while ultra-fine (< 1–2nm) copper oxide clusters stay on the ceria support.

From Fig. 3a and 3b, with the help of various standards of copper (Cu foil for Cu^0, Cu_2O for Cu^+ and CuO for Cu^{2+}) and palladium (Pd foil for Pd^0 and PdO for Pd^{2+}), we have done the liner combination fits on XANES profiles (see details in Fig. S2). Fully oxidized copper species (Cu^{2+}), without any fraction of reduced components of

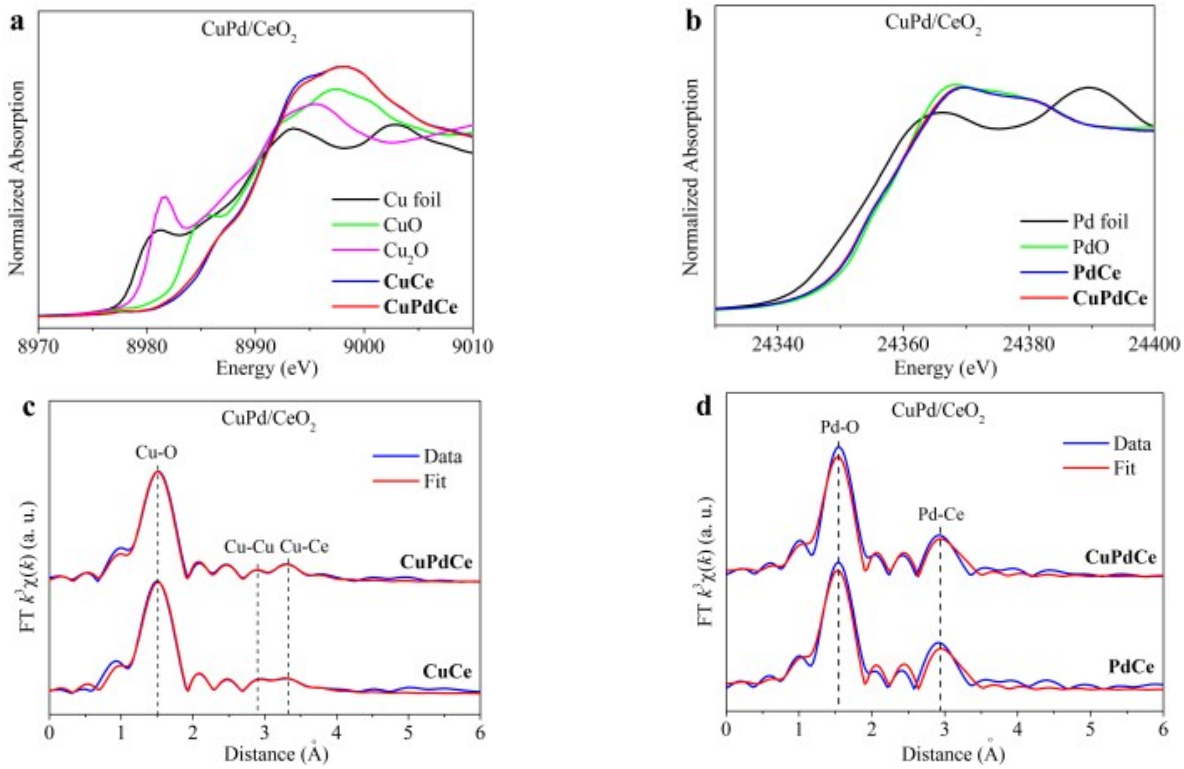

Fig. 3 (a,b) XANES profiles and (c,d) EXAFS spectra with fits of ceria-supported copper-palladium oxides: (a,c) Cu K-edge; (b,d) Pd K-edge.

Table 2. EXAFS fitting results of ceria-supported copper-palladium oxide clusters.[a]

Shell	CuCe		PdCe		CuPdCe	
	R (Å)	CN	*R* (Å)	CN	*R* (Å)	CN
Cu-O	1.94±0.03	4.0±0.2	—	—	1.94±0.03	4.0±0.3
Pd-O	—	—	2.00±0.01	4.6±0.4	2.00±0.01	4.7±0.3
Cu-Cu	3.23±0.03	0.6±0.3	—	—	3.24±0.04	0.4±0.2
Cu-Ce	3.45±0.03	0.7±0.3	—	—	3.46±0.02	0.8±0.2
Pd-Ce	—	—	3.22±0.02	2.7±0.8	3.21±0.02	2.5±0.7

[a] ΔE_0 = 1.6±0.4 eV or 4.2±0.5 eV for all the analyzed Cu or Pd shells.

View Article Online
DOI: 10.1039/C6QI00535G

Cu^{+}/Cu^{0}, were identified for both **CuCe** and **CuPdCe**. On the other hand, the molar ratios between Pd^{0}/Pd^{2+} were very close between **PdCe** (14/86) and **CuPdCe** (16/84).Therefore, identical oxidation states of both copper and palladium were detected for bimetallic oxides and single metal oxides. This is also in good agreement with the similar binding energies in Cu 2p and Pd 3d XPS spectra (see details in Fig. S3). Furthermore, from Fig. 3a, we found the obvious discrepancies in the range of 8980–9000 eV between CuO and **CuCe/CuPdCe**, because of the presence of ultra-fine (< 1–2 nm) copper oxide clusters and metal-support interaction[17] in the as-calcined samples, which exhibit totally different XANES profiles other than the bulk CuO reference. On the basis of EXAFS fitting results (Fig. 3c and 3d, Table 2), we obtained the following conclusions on our ceria-supported copper-palladium oxide clusters.

(1) A strong peak at 1.94 Å (CN = 4.0) or 2.00 Å (CN = 4.6–4.7) was identified for the first shell of Cu K-edge (CuCe and CuPdCe) or Pd K-edge (**PdCe** and **CuPdCe**), respectively, which is contributed by the Cu-O_x or Pd-O_x species. The fitted *R* and CN values are very close to those of ceria-supported highly dispersed copper oxide[10,17] or palladium oxide clusters.[20]

(2) Weak peaks of longer distances (2.7–3.5 Å) and lower coordination numbers (< 3) appeared for the second shells. For Cu K-edge (**CuCe** and **CuPdCe**), both Cu-Cu (*R* = 3.23–3.24 Å; CN = 0.4–0.6) and Cu-Ce (*R* = 3.45–3.46 Å; CN = 0.7–0.8) can be verified; while for Pd K-edge (**PdCe** and **CuPdCe**), only Pd-Ce (*R* = 3.21–3.22 Å; CN = 2.5–2.7) can be identified. These results confirmed that both metal-support interaction (Cu-O_x-Ce) and the internal correlation of copper oxide clusters (Cu-O_x-Cu) are present for **CuCe** or **CuPdCe**;[10] while only the metal-support interaction (Pd-O_x-Ce) exists in **PdCe** and **CuPdCe**.[20]

(3) No direct metal-metal bonds (Cu-Cu and Pd-Pd) were determined, which is in good agreement with the fully oxidized copper (Cu^{2+}) and palladium (Pd^{2+}) species in XANES. Furthermore, no direct bond between bimetallic oxide components (Cu-O_x-Pd) was found, which gives a hint that both copper and palladium species are separately dispersed on the surface of ceria nanorods.

(4) No new contributions were detected for the bimetallic oxides (**CuPdCe**), if compared to the corresponding single metal oxides (**CuCe** and **PdCe**). All the fitted values for copper-palladium oxides (**CuPdCe**, Cu K-edge and Pd K-edge) are identical to the simple sum of those for both copper oxide (**CuCe**, Cu K-edge) and palladium oxide (**PdCe**, Pd K-edge).

CO oxidation reaction ($2CO + O_2 = 2CO_2$) was used to evaluate the catalytic performance of ceria-supported copper-palladium oxide clusters. The "light off" profiles in Fig. 4a under transient mode clearly display the higher CO conversions of Pd-containing samples (**PdCe** and **CuPdCe**), compared to those of Pd-free counterpart (**CuCe**). From Fig. 4b, we can see that the CO conversions for all the measured catalysts were nearly unchanged throughout the stability tests. The reactivity of different copper-palladium oxides follows this sequence: **CuPdCe** (88%) ≈ **PdCe** (81%) > **CuCe** (55%). Thus, on the basis of these results, we can verify that the catalytic performance of bimetallic oxide clusters (**CuPdCe**) is slightly superior to that of single palladium oxide counterpart (**PdCe**), and copper component shows very limited effect on the reactivity.

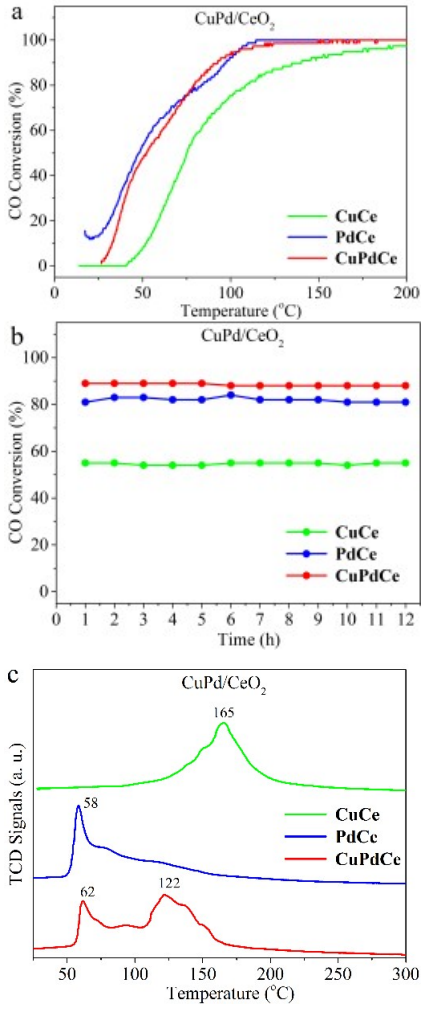

Figure 4. (a) "Light off", (b) stability at 80 °C and (c) H_2-TPR profiles of ceria-supported copper-palladium oxides for the CO oxidation reaction.

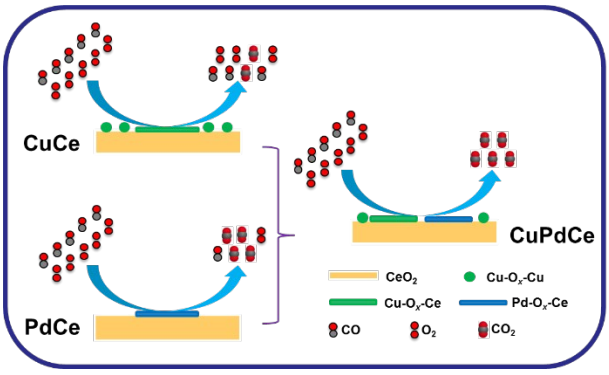

Scheme 1. Structural demonstration on ceria-supported copper-palladium oxide clusters.

In order to reveal the metal-support interaction between copper-palladium species and ceria nanorods, H_2-TPR was applied over the fresh samples. Fig. 4c shows a broad band at ca. 165 °C for **CuCe**, which was shifted to a lower temperature of 122 °C for **CuPdCe**, probably due to the strength change of highly dispersed CuO_x clusters and Cu-O_x-Ce species. However, for active palladium-containing catalysts, the sharp reduction peak around 60 °C, which can be attributed to the Pd-O_x-Ce contribution, was almost constant between bimetallic oxides (**CuPdCe**) and single metal oxide (**PdCe**).

By the aids of multiple characterization techniques, we now have a full view on the local coordination structure of ceria-supported copper-palladium oxide clusters (see Scheme 1). First, for the current single copper oxide clusters (**CuCe**), the related HAADF-STEM images determine the subnanometer (< 1–2 nm) copper species across ceria nanorods (Fig. 2d). The XANES profiles identify the fully oxidized Cu^{2+} state (Figure 3a), and the EXAFS fitting results verify the presence of both Cu-O_x-Cu species (see the green dots in Scheme 1) from the highly dispersed CuO_x clusters and Cu-O_x-Ce species (see the green bar in Scheme 1) from the metal-support interaction (also confirmed by H_2-TPR) between copper and ceria (Fig. 3c). Copper-ceria catalyst is not very active for low-temperature CO oxidation reaction, and the single copper oxide clusters supported on CeO_2 nanorods exhibit the lowest CO conversion among all the three samples (Fig. 4a and 4b).

Second, for our palladium oxide clusters (**PdCe**), the HAADF-STEM images confirm the homogenous distribution of palladium species over the CeO_2 support at the atomic scale (Fig. 2e). The XANES profiles identify the highly oxidized Pd^{2+} state (Fig. 3b), and the EXAFS fitting results, together with the H_2-TPR data, verify the existence of single Pd-O_x-Ce species (see the blue bar in Scheme 1) from the metal-support interaction between palladium and ceria (Fig. 3d). Palladium-ceria catalyst is active for low-temperature CO oxidation reaction, and the single palladium oxide clusters supported on ceria nanorods display much higher reactivity for the CO oxidation than the single copper oxide clusters (Fig. 4a and 4b).

However, unlike the reported synergistic effect[12,13] on the catalytic performance of oxide-supported bimetallic oxide catalysts, our ceria-supported bimetallic copper-palladium oxide clusters (**CuPdCe**) did not behave distinctly higher reactivity to the active single metal oxide (**PdCe**) clusters, according to the experimental data from "light off" profiles in Fig. 4a and constant CO conversions in Fig. 4b. Despite the possibility of miscible alloys between copper and palladium metals (Cu_xPd_{1-x}), we found that the fully oxidized Cu^{2+} and highly oxidized Pd^{2+} species are unable to form Cu-O_x-Pd bond via the bridged oxygen atoms. Actually, on the basis of EXAFS fitting results, the local coordination structure for copper-palladium oxide clusters can be regarded as the simple sum of two single metal oxide clusters geometrically (Table 2, also see Scheme 1). Furthermore, the H_2-TPR data show that the critical reduction peak by Pd-O_x-Ce interaction was unchanged after the introduction of secondary copper oxide component (Fig. 4c). Therefore, it is reasonable that no synergistic effect on the catalytic performance of copper-palladium oxide clusters demonstrated in this work. Considering the enhanced CO conversion during oxygen-assisted water-gas shift (WGS) reaction for the ceria-supported Cu-Pd bimetallic catalyst via wetness impregnation, synthesized by Song's group[13], we believe such conclusion of no synergistic effect is actually case specific for our deposition-precipitation synthesis, as well as the low-temperature CO oxidation reaction.

Conclusions

In summary, bimetallic copper-palladium oxide clusters supported on the surfaces of ceria nanorods have been prepared by a two-step deposition-precipitation approach. With the help of multiple characterization approaches including HAADF-STEM and XAFS, we have identified that both copper and palladium species are fully oxidized (Cu^{2+} and Pd^{2+}) in the form of Cu-O_x-Ce and Pd-O_x-Ce, which strongly interact with the CeO_2 support. Also, the Cu-O_x-Cu structure was verified for copper oxide clusters only. No direct bond between bimetallic oxides (Cu-O_x-Pd) was detected, and thus no synergistic effect on the catalytic activity of ceria-supported copper-palladium oxide clusters was demonstrated for the CO oxidation reaction.

Experimental

Materials

All the chemicals used in this work were of analytical grade and purchased from Sinopharm Chemical Reagent Co., Ltd without any further purification.

Synthesis

Preparation of ceria nanorods: The ceria nanorods were synthesized according to the hydrothermal method[21]. $Ce(NO_3)_3{\cdot}6H_2O$ (4.5 mmol) was added into an aqueous NaOH (6 M, 60 mL) solution under vigorous stirring. After the precipitation process was completed (about 10 min), the stock solution was transferred into a Teflon bottle, and further tightly sealed in a stainless-steel autoclave. The hydrothermal procedure was carried out in a temperature-controlled electric oven at 100 °C for 24 h. The precipitates were separated by centrifugation and then washed by deionized water four times and ethanol once. The ceria support was obtained by drying the as-washed product in air under 70 °C overnight.

Deposition of copper-palladium oxide clusters: Ceria-supported copper-palladium oxide clusters samples were synthesized via a deposition-precipitation method. $Cu(NO_3)_2{\cdot}2.5H_2O$ (0.3 mmol), K_2PdCl_4 (0.1 mmol) and as-calcined CeO_2 nanorods (1 g) were suspended in 100 mL Millipore (> 18 MΩ) water under vigorously stirring. Then, Na_2CO_3 aqueous solution (0.5 M) were dropped into the above solution until the final pH value of ~ 9. After the generation of greenish slurries, the stock solution was further aged at 80 °C for another 4 h. The as-obtained precipitates were filtered and then washed by Millipore (> 18 MΩ·cm) water for three Times. The as-washed powders were dried in vacuum at 80 °C overnight and then calcined in still air at 500 °C for 4 h (ramping rate: 2 °C/min).

Characterizations

View Article Online
DOI: 10.1039/C6QI00536C

The bulk concentrations of copper (Cu_{bulk} in at.%) and palladium (Pd_{bulk} in at.%) were determined by inductively coupled plasma atomic emission spectroscopy (ICP-AES) on an IRIS Intrepid II XSP instrument (Thermo Electron Corporation).

The X-ray photoelectron spectroscopy (XPS) analysis was performed on an Axis Ultra XPS spectrometer (Kratos, U.K.) with 225 W of Al Kα radiation. The C 1s line at 284.8 eV was used to calibrate the binding energies. The surface concentrations of copper (Cu_{surf} in at.%) and palladium (Pd_{surf} in at. %) were determined by integrating the areas of Cu 2p, Pd 3d and Ce 3d peaks in the CasaXPS software.

Raman spectra were acquired by excitation of the sample at 532 nm using a Raman microscope system (HORIBA JOBIN YVON) in the spectral window from 100 to 800 cm^{-1} with a resolution of 2 cm^{-1}.

The powder X-ray diffraction (XRD) patterns were recorded on a Bruker D8 Advance diffractometer (40 kV, 40 mA) with a scanning rate of 4 ° min^{-1}, using Cu Kα1 radiation (λ = 1.5406 Å). The diffraction patterns were collected from 20 to 70 ° with a step of 0.02 °. The 2θ angles were calibrated with a μm-scale Alumina disc. The powder sample after grinding was placed inside a quartz sample holder for each test. With the software "LAPOD" of least-squares refinement of cell dimensions of cubic CeO_2 from powder data by Cohen's method[22,23].

The nitrogen adsorption-desorption measurements were performed on an ASAP2020-HD88 analyzer (Micromeritics Co. Ltd.) at 77 K. The measured powders were degassed at 150 °C under vacuum (< 100 μmHg) for over 4 h. The BET specific surface areas (S_{BET}) were calculated from data in the relative pressure range between 0.05 and 0.20.

Electron microscopy

The aberration-corrected high-angle annular dark-field scanning transmission electron microscopy (HAADF-STEM) images, together with the corresponding X-ray energy dispersive spectroscopy (EDS) were carried out on the JEOL ARM200F microscope equipped with probe-forming spherical-aberration corrector. Due to the high Z of the Ce atoms (Z = 58), the contrast of Pd (Z = 46) and Cu (Z = 29) small clusters (less than 1 nm) in HAADF images is almost invisible, particularly for the thick region. Here, the EDS elemental mapping was performed to identify the distribution of Cu and Pd clusters in CeO_2 nanorods. The inner and outer angles of the HAADF detector were set at 90 and 370 mrad, respectively, and the convergence angle at 30 mrad. The spherical aberration coefficient of the condense lens was set to 0.5 μm. In this image condition, the spatial resolution of HAADF images is about 0.08 nm.

X-ray absorption fine structure

The X-ray absorption fine structure (XAFS) spectra at Cu K (E_0 = 8979 eV) and Pd K (E_0 = 24350 eV) edges were performed at BL14W1 beamline[24] of Shanghai Synchrotron Radiation Facility (SSRF) operated at 3.5 GeV under "top-up" mode with a constant current of 220 mA. The XAFS data were recorded under fluorescence mode with a standard Lytle ion chamber and a 32-element Ge solid state detector for Cu and Pd, respectively. The energy was calibrated accordingly to the absorption edge of pure Cu and Pd foil.

Athena and Artemis codes were used to extract the data and fit the profiles. For the X-ray absorption near edge structure (XANES) part, the experimental absorption coefficients as function of energies $\mu(E)$ were processed by background subtraction and normalization procedures, and reported as "normalized absorption". Based on the normalized XANES profiles, the molar fraction of $Cu^{2+}/Cu^{+}/Cu^{0}$ and Pd^{2+}/Pd^{0} can be determined by the linear combination fit[25].

For the extended X-ray absorption fine structure (EXAFS) part, the Fourier transformed (FT) data in R space were analyzed by applying first shell approximation model for Cu-O/Pd-O, Cu-Cu and Cu-Ce/Pd-Ce contributions. The passive electron factors, S_0^2, were determined by fitting the experimental data on Cu and Pd foils and fixing the coordination number (CN) of Cu-Cu and Pd-Pd to be 12, and then fixed for further analysis of the measured samples. The parameters describing the electronic properties (e.g., correction to the photoelectron energy origin, E_0) and local structure environment including CN, bond distance (R) and Debye-Waller (D.W.) factor around the absorbing atoms were allowed to vary during the fit process. The fitted ranges for k and R spaces were selected to be k = 2.8–11.0 $Å^{-1}$ with R = 1.1–4.2 (Cu-O, Cu-Cu and Cu-Ce) Å (k^3 weighted) and k = 3–11.5 $Å^{-1}$ with R = 1.0–3.4 (Pd-O and Pd-Ce) Å (k^3 weighted), respectively. To distinguish the effect of Debye-Waller factor from coordination number, we set σ^2 to be 0.004 and 0.008 for all the analysed M-O (M = Cu, Pd) and M-M (M = Cu, Pd, Ce) shells.

Catalytic tests

The temperature-programmed reduction by hydrogen (H_2-TPR) was performed in a Builder PCSA-1000 instrument equipped with a thermal conductivity detector (TCD). The reduction process was carried out in a mixture of 5% H_2/Ar (30 mL/min) from room-temperature to 400 °C (5 °C min^{-1}). The sieved catalysts (40~60 mesh, 30 mg) were pretreated in pure O_2 at 300 °C for 30 min before each test.

The CO oxidation activities for ceria-supported copper-palladium oxide clusters samples were evaluated in a plug flow reactor using 50 mg of sieved (40–60 mesh) powders in a gas mixture of 1 vol.% CO, 20 vol.% O_2 and 79 vol.% N_2 (from Jinan Deyang Corporation, 99.997% purity) at a flow rate of 67 mL/min, corresponding to a space velocity of 80,000 $mL \cdot h^{-1} g_{cat}^{-1}$. Prior to the test, the catalysts were pretreated in air at 300 °C for 30 min for activation. After the catalysts cooled down to room temperature under a flow of pure N_2 gas, reactant gases was passed through the reactor. The "light off", ignition of CO oxidation reaction, profiles were obtained in a transient mode with significant changes of CO conversions in the range of ca. 20 to 200 °C with a ramping rate of 3 °C/min. The related stability tests were done in the same conditions at the constant reaction temperature of 80 °C for 12 h. The outlet gas compositions of CO and CO_2 were monitored online by a non-dispersive IR spectroscopy (Gasboard 3500, Wuhan Sifang

Company, China). The CO conversion was calculated according to the following equations: CO conversion (%) = ($CO_{in} - CO_{out}$) / $CO_{in} \times 100$.

Acknowledgements

This work was supported by the National Science Foundation of China (NSFC) (grant nos. 21373259, 21301107, 11405256 and 11079005), the Excellent Young Scientists Fund from the NSFC (21622106), the Hundred Talents project of the Chinese Academy of Sciences, the Strategic Priority Research Program of the Chinese Academy of Sciences (grant no. XDA09030102), the Taishan Scholar project of Shandong Province (China), Open Funding from Beijing National Laboratory for Molecular Science and Open Funding from Key Laboratory of Interfacial Physics and Technology, Chinese Academy of Sciences.

Notes and references

1 A. A. Herzing, C. J. Kiely, A. F. Carley, P. Landon, G. J. Hutchings, *Science*, 2008, **321**, 1331−1335.
2 Y. Lei, F. Mehmood, S. Lee, J. Greeley, B. Lee, S. Seifert, R. E. Winans, J. W. Elam, R. J. Meyer, P. C. Redfern, D. Teschner, R. Schlögl, M. J. Pellin, L. A. Curtiss, S. Vajda, *Science*, 2010, **328**, 224−228.
3 M. Yang, S. Li, Y. Wang, J. A. Herron, Y. Xu, L. F. Allard, S. Lee, J. Huang, M. Mavrikakis, M. Flytzani-Stephanopoulos, *Science*, 2014, **346**, 1498−1501.
4 Y.-P. Zhai, D. Pierre, R. Si, W.-L. Deng, P. Ferrin, A. U. Nilekar, G. Peng, J. A. Herron, D. C. Bell, H. Saltsburg, M. Mavrikakis, M. Flytzani-Stephanopoulos, *Science*, 2010, **329**, 1633−1637.
5 J. Ke, W. Zhu, Y.-Y. Jiang, R. Si, Y. J. Wang, S.-C. Li, C.-H. Jin, H.-C. Liu, W.-G. Song, C.-H. Yan, Y.-W. Zhang, *ACS Catal.*, 2015, **5**, 5164−5173.
6 E. M. Slavinskaya, R. V. Gulyaev, A. V. Zadesenets, O. A. Stonkus, V. I. Zaikovskii, Y. V. Shubin, S. V. Korenev, A. I. Boronin, *Appl. Catal. B*, 2015, **166/167**, 91–103.
7 Z. Hu, X.-F. Liu, D.-M. Meng, Y. Guo, Y.-L. Guo, G.-Z. Lu, *ACS Catal.*, 2016, **6**, 2265−2279.
8 Q. Yang, X.-P. Fu, C.-J. Jia, C. Ma, X. Wang, J. Zeng, R. Si, Y.-W. Zhang, C.-H. Yan, *ACS Catal.*, 2016, **6**, 3072−3082.
9 M. Manzolia, R. D. Monteb, F. Boccuzzia, S. Colucciaa, J. Kašparb, *Appl. Catal. B*, 2005, **61**, 192–205.
10 W.-W. Wang, P.-P. Du, S.-H. Zou, H.-Y. He, R.-X. Wang, Z. Jin, S. Shi, Y.-Y. Huang, R. Si, Q.-S. Song, C.-J. Jia, C.-H. Yan, *ACS Catal.*, 2015, **5**, 2088–2099.
11 C. J. Heard, S. Vajda, R. L. Johnston, *J. Phys. Chem. C*, 2014, **118**, 3581-3589.
12 J. Kugai, J. T. Miller, N. Guo, C. S. Song, Catalysts. *J. Catal.*, 2011, **277**, 46–53.
13 J. Kugaia, E. B. Fox, C. S. Song, *Appl. Catal. A*, 2013, **456**, 204–214.
14 B.-W. Lu, Y.-W. Ju, T. Abe, K. Kawamoto, *Inorg. Chem. Front.*, 2015, **2**, 741–748.
15 R. Si, M. Flytzani-Stephanopoulos, *Angew. Chem. Int. Ed.*, 2008, **47**, 2884–2887.
16 R. Si, J. Raitano, N. Yi, L.-H. Zhang, S.-W. Chan, M. Flytzani-Stephanopoulos, *Catal. Today* 2012, **180,** 68–80.
17 P.-P. Du, W.-W. Wang, C.-J. Jia, Q.-S. Song, Y.-Y. Huang, R. Si, *Appl. Catal. A*, 2016, **518**, 87–101.
18 Y. Lee, G.-H. He, A. J. Akey, R. Si, M. Flytzani-Stephanopoulos, I. P. Herman, *J. Am. Chem. Soc.*, 2011, **133**, 12952–12955.
19 H.-X. Mai, L.-D. Sun, Y.-W. Zhang, R. Si, W. Feng, H.-P. Zhang, H.-C. Liu, C.-H. Yan, *J. Phys. Chem. B*, 2005, **109**, 24380–24385.
20 K. R. Priolkar, P. Bera, P. R. Sarode, M. S. Hegde, S. Emura, R. Kumashiro, N. P. Lalla, *Chem. Mater.*, 2002, **14**, 2120–2128.
21 H.-X. Mai, L.-D. Sun, Y.-W. Zhang, R. Si, W. Feng, H.-P. Zhang, H.-C. Liu, C.-H. Yan, *J. Phys. Chem. B* 2005, **109**, 24380-24385.
22 J. I. Langford, *J. Appl. Cryst.* 1971, **4**, 259-260.
23 J. I. Langford, *J. Appl. Cryst.* 1973, **6**, 190-196.
24 H.-S. Yu, X.-J. Wei, J. Li, S.-Q. Gu, S. Zhang, L.-H. Wang, J.-Y. Ma, L.-N. Li, Q. Gao, R. Si, F.-F. Sun, Y. Wang, F. Song, H.-J. Xu, X.-H. Yu, Y. Zou, J.-Q. Wang, Z. Jiang, Y.-Y. Huang, *Nucl. Sci. Tech.* 2015, **26**, 050102.
25 A. I. Frenkel, Q. Wang, N. Marinkovic, J.-G. Chen, L. Barrio, R. Si, A. Lopez Camara, A. M. Estrella, J. A. Rodriguez, J. C. Hanson, *J. Phys. Chem. C* 2011, **115**, 17884-17890.